Polymorphism and its effects on the magnetic behaviour of the [Fe(sal$_2$-trien)][Ni(dmit)$_2$] spin-crossover complex†

Christophe Faulmann,* Petra Á. Szilágyi, Kane Jacob, Joe Chahine and Lydie Valade

Received (in Montpellier, France) 17th March 2009, Accepted 30th April 2009
First published as an Advance Article on the web 11th May 2009
DOI: 10.1039/b901779h

The syntheses, structural characterisation, and magnetic and spectroscopic properties of three new polymorphs of the spin-crossover complex [Fe(sal$_2$-trien)][Ni(dmit)$_2$] are reported. The results are discussed as a function of their intra- and intermolecular arrangement. Correlation of their crystal structures and magnetic properties suggest that some torsion angles play a significant role in the magnetic properties of this class of compounds. Intermolecular contacts are also of importance, and the nature of the short contacts between molecular species seems to be more crucial than their number in the allowance of spin-crossover.

Introduction

Fe spin-crossover (SCO) complexes are of current interest from a fundamental point of view,[1–7] as well as for their potential applications as functional materials in sensor and memory device design and fabrication.[8–12] These complexes may be reversibly switched between two electronic configurations, low-spin (LS) and high-spin (HS). This switching can be induced by external effects, such as temperature, pressure, light irradiation, pulsed magnetic field and even analytes (typically solvent molecules). The two states reveal differences in magnetism, optical and dielectric constant properties, as well as in their crystal structures. Furthermore, strong elastic interactions between the metal ions may give rise to a first-order phase transition with hysteresis (memory effect) between the HS and LS forms.

Electrical conductivity is a fundamental material property that has been investigated in the domain of molecular science.[13] $(NR_4)[M(dmit)_2]_x$ ($x > 1$)-type compounds with non-integral oxidation states display interesting electron transport properties ($dmit^{2-}$: 2-thioxo-1,3-dithiole-4,5-dithiolato). Combining SCO and electrical conductivity was the aim of Dorbes *et al.*[14] when they first synthesised the 1 : 1 complex [Fe(sal$_2$-trien)][Ni(dmit)$_2$] (sal$_2$-trien is the ligand formed from the condensation of two molecules of salicylaldehyde (sal) with triethylenetetramine (trien)), a precursor of the fractional oxidation state complex [Fe(sal$_2$-trien)][Ni(dmit)$_2$]$_3$.[15] Analogously, similar properties have been studied in the salts of $[Fe(qsal)_2]^+$ and Fe(R-salEen)]$^+$ complex cations too (qsalH and salEen stand for *N*-(8-quinolyl)-salicylaldimine and *N*-((2-ethylamino)ethyl)-salicylaldimine, respectively, with R = H, CH_3O).[16–22]

The crystal structure and magnetic properties of the above-mentioned [Fe(sal$_2$-trien)][Ni(dmit)$_2$] SCO complex, was reported in ref. 14. This complex will be referred to as *t*-**1**.

Since complex **1** is not of fractional oxidation state, it does not exhibit electrical properties. However, it undergoes a complete spin transition with a hysteresis loop centred around 245 K. Such a feature is rarely observed in Fe(III) complexes.[23] In order to synthesize larger amounts of **1** for further physical studies, the same synthetic procedure was applied, but surprisingly, only four novel phases of [Fe(sal$_2$-trien)][Ni(dmit)$_2$] were obtained, which were polymorphs (or pseudo-polymorphs) of that obtained previously. These new phases crystallized either during direct synthesis or after re-crystallization. It has to be noted here that despite our efforts, we were unable to re-synthesize the "original" triclinic phase. Whatever the experimental conditions (reaction or re-crystallization temperature, solvent, concentration, *etc.*..) and quality of reactants (raw or re-crystallized), only the new polymorphs have been obtained so far. Thus, up to now, the "native" *t*-**1** phase could not be re-synthesized, whatever method was used to re-prepare it. Such an event is not uncommon, as illustrated in the literature.[24–26]

Here, we report the syntheses, variable-temperature structural characterization, magnetic and spectroscopic properties, and theoretical aspects of these four new phases, two of which are monoclinic and two of which are triclinic. For reasons of clarity, they will be abbreviated to *m*-**1**, *m*-**1′**, *t*-**1′** and *t*-**1″**, respectively. The "native" triclinic form (with the hysteresis loop) will be abbreviated *t*-**1**.

The two monoclinic forms are real polymorphs of *t*-**1**, with the chemical formula [Fe(sal$_2$-trien)][Ni(dmit)$_2$] (*m*-**1**, *m*-**1′**). The triclinic forms (*t*-**1′** and *t*-**1″**) are pseudo-polymorphs, since they are solvated; their chemical formula is [Fe(sal$_2$-trien)][Ni(dmit)$_2$]·$(CH_3)_2CO$·CH_3CN and [Fe(sal$_2$-trien)]-[Ni(dmit)$_2$]$(CH_3)_2CO$ (*t*-**1″**), respectively.‡

Laboratoire de Chimie de Coordination-CNRS 205, Route de Narbonne, F-31077, Toulouse, France.
E-mail: christophe.faulmann@lcc-toulouse.fr; Fax: +33 56155 3003; Tel: +33 56133 3100

† Electronic supplementary information (ESI) available: Fig. S1, Tables S1–S5. CCDC reference numbers 729925–729931. For ESI and crystallographic data in CIF or other electronic format see DOI: 10.1039/b901779h

‡ During the preparation of this manuscript, another pseudo-polymorph was obtained: [Fe(sal$_2$-trien)]$_2$[Ni(dmit)$_2$]$_2$·$(CH_2Cl_2)_2$ (*t*-**1‴**). Triclinic, space group $P\bar{1}$, with a = 13.704(2), b = 16.1815(19), c = 19.248(3) Å, α = 111.346(14), β = 95.298(16), γ = 106.786(15)° and V = 3711.6(8) Å^3 at 260 K. Its crystal structure will be reported later.

Results

Crystal structure description

The cell parameters, together with several X-ray data parameters, are summarized in Table 1. All compounds, *m*-**1**, *m*-**1′**, *t*-**1′** and *t*-**1″**, contain the $[Fe(sal_2\text{-trien})]^+$ and $[Ni(dmit)_2]^-$ units in a 1 : 1 ratio. *t*-**1′** also contains one CH_3CN and one $(CH_3)_2CO$ molecule, and *t*-**1″** contains one $(CH_3)_2CO$ molecule. The labelling of the asymmetric units of the three polymorphs can be seen in Fig. 1 and Fig. 2.

The main difference between the four phases containing the $[Fe(sal_2\text{-trien})]^+$ and $[Ni(dmit)_2]^-$ units lies in their structural arrangement. It should be mentioned that there are a few intramolecular discrepancies within the bond lengths and angles at corresponding temperature values. These differences will only be discussed in detail in the case of *t*-**1** and *m*-**1** (*vide infra*). The structure of *t*-**1** has been described previously.[14] At room temperature and 180 K, it is built up of slabs of $[Fe(sal_2\text{-trien})]^+$ cations and layers of $[Ni(dmit)_2]^-$ anions that alternate along the c-axis and spread out over the ab plane (Fig. 3).

The asymmetric unit of *m*-**1** contains one $[Fe(sal_2\text{-trien})]^+$ cation and one $[Ni(dmit)_2]^-$ anion (Fig. 1). The structure of *m*-**1** has been determined at 293 and 180 K, and compared to that of *t*-**1**. Like the structure of *t*-**1**, the structure of *m*-**1** can be described as double layers of $[Ni(dmit)_2]^-$ units separated from each other by a double layer of $[Fe(sal_2\text{-trien})]^+$

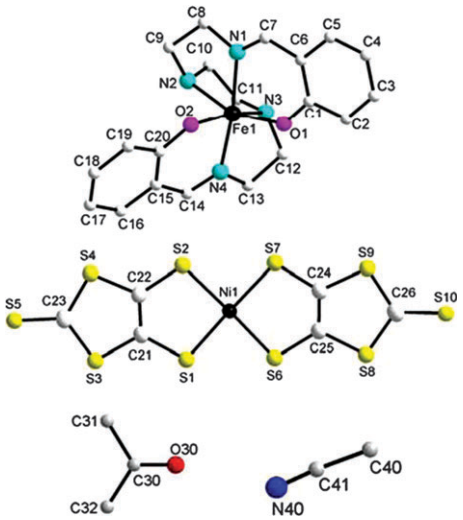

Fig. 1 Labelling for *m*-**1** (Fe and Ni moieties), for *t*-**1′** (Fe, Ni, $(CH_3)_2CO$ and CH_3CN moieties) and for *t*-**1″** (Fe, Ni, and $(CH_3)_2CO$ moieties).

Table 1 Summary of X-ray data collection and refinement for *m*-**1**, *m*-**1′**, *t*-**1′** and *t*-**1″**

	m-**1**		*m*-**1′**		*t*-**1′**		*t*-**1″**
	$[Fe(sal_2\text{-trien})][Ni(dmit)_2]$		$[Fe(sal_2\text{-trien})][Ni(dmit)_2]$		$[Fe(sal_2\text{-trien})][Ni(dmit)_2]\cdot(CH_3)_2CO\cdot CH_3CN$		$[Fe(sal_2\text{-trien})][Ni(dmit)_2]\cdot(CH_3)_2CO$
Diffractometer	Oxford Xcalibur	IPDS STOE	Bruker Apex2		IPDS STOE	Oxford Xcalibur	IPDS STOE
Empirical formula	$C_{26}H_{24}FeN_4NiO_2S_{10}$		$C_{26}H_{24}FeN_4NiO_2S_{10}$		$C_{31}H_{33}FeN_5NiO_3S_{10}$		$C_{29}H_{30}FeN_4NiO_3S_{10}$
M_r	859.65		859.65		958.78		917.73
T/K	180(2)	293(2)	160(2)	295(2)	100(2)	250(2)	293(2)
Crystal system	Monoclinic		Monoclinic		Triclinic		Triclinic
Space group	$P2_1/c$		$C2/c$		$P\bar{1}$		$P\bar{1}$
a/Å	17.4443(8)	17.589(2)	44.9352(18)	45.169(1)	11.825(5)	11.8510(6)	11.929(2)
b/Å	10.6294(5)	10.7316(8)	13.5827(5)	13.7916(3)	12.542(5	12.6497(5)	12.080(2)
c/Å	17.7187(8)	17.774(1)	22.5430(10)	22.6893(6)	13.795(5)	13.9373(7)	16.541(2)
α (°)	90	90	90	90	106.884(5)	106.764(4)	111.18(2).
β (°)	101.511(4)	101.342(9)	104.386(2)	104.541(1)	90.945(5)	90.695(4)	76.94(2)
γ (°)	90	90	90	90	93.107(5)	92.602(4)	115.27(1)
V/Å^3	3219.4(3)	3289.5(4)	13327.5(9)	13681.6(6)	1953.7(1)	1997.8(2)	2002.5(5)
Z	4		16		2		2
D_c/g cm^{-3}	1.774	1.736	1.714	1.669	1.630	1.594	1.522
F(000)	1752		7008		984		940
μ/mm^{-1}	1.719	1.683	1.661	1.618	1.630	1.397	1.389
θ range for data collection/°	3.08–32.29	2.23–25.98	0.94–31.28	0.93 to 26.78	2.28 to 25.79	3.03 to 32.00	1.89–24.12
No. reflections collected	37828	45235	92000	83938	18822	21275	16210
No. independent reflections	10845	6410	21408	14573	6964	12574	5975
R_{int}	0.0585	0.0649	0.0289	0.0277	0.0731	0.0203	0.1113
No. data/ restraints/ parameters	10845/0/397	6410/0/397	21408/0/798	14573/0/798	6964/0/463	12574/0/463	5975/0/435
Goodness of fit on F^2	1.020	0.956	1.022	1.036	0.977	1.082	0.933
Final R indices $[I > 2\sigma(I)]$	R_1 = 0.0579	R_1 = 0.0292	R_1 = 0.0423	R_1 = 0.04570	R_1 = 0.0504	R_1 = 0.0377	R_1 = 0.0515
	wR_2 = 0.1111	wR_2 = 0.0635	wR_2 = 0.1037	wR_2 = 0.1238	wR_2 = 0.1246	wR_2 = 0.0961	wR_2 = 0.1439
R indices (all data)	R_1 = 0.0579	R_1 = 0.0465	R_1 = 0.0749	R_1 = 0.0870	R_1 = 0.0807	R_1 = 0.0769	R_1 = 0.0837
	wR_2 = 0.1111	wR_2 = 0.0670	wR_2 = 0.1323	wR_2 = 0.1641	wR_2 = 0.1361	wR_2 = 0.1217	wR_2 = 0.1535
$H_{max,min}$/e Å^3	1.341 & −0.609	0.297 & −0.370	1.290 & −0.874	0.591 & −0.391	0.675 & −0.887	0.816 & −0.622	1.069 & −0.374

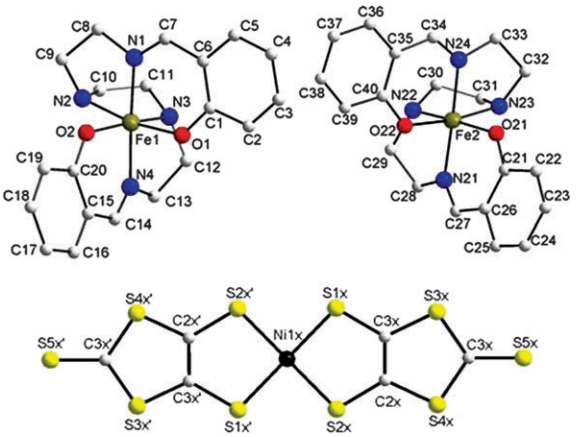

Fig. 2 Labelling for the two $[Fe(sal_2\text{-trien})]^+$ cations and the $[Ni(dmit)_2]^-$ anion in the asymmetric unit of *m*-**1**′ (x stands for A, B, C and D).

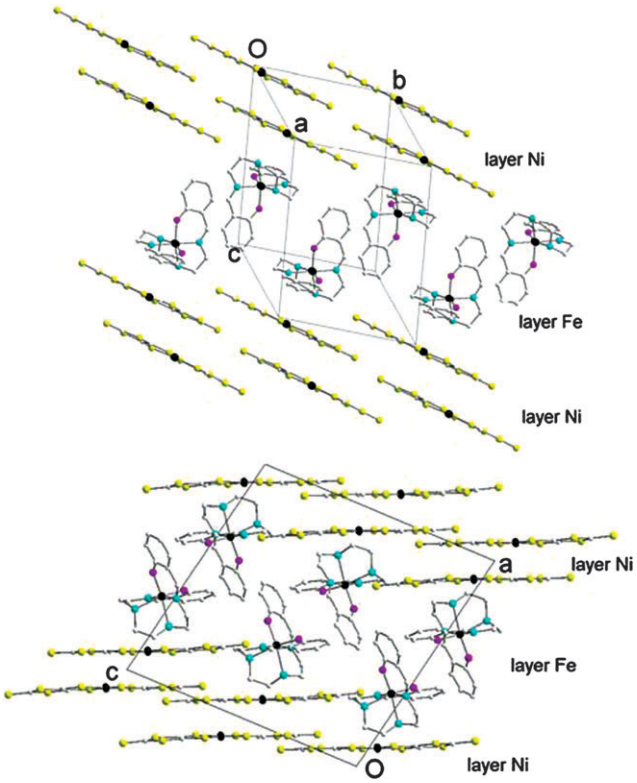

Fig. 3 Projection of the structure of *t*-**1** (top) and *m*-**1** (bottom) in their HS state.

cations, each layer spreading out over the bc plane (Fig. 3). The same arrangement of ferric units in the two polymorphs could be assumed, unless a closer look is taken at their structures. The intramolecular geometry, together with the structural arrangement, will be discussed in detail later in this paper.

The asymmetric unit of *m*-**1**′ contains two $[Fe(sal_2\text{-trien})]^+$ units and four half units of $[Ni(dmit)_2]^-$ anions (Fig. 2). Three Ni atoms (Ni1A, Ni1C and Ni1D) are located on a symmetry centre and the fourth (Ni1B) lies on a second-order axis. The structural arrangement of *m*-**1**′ can be described as layers

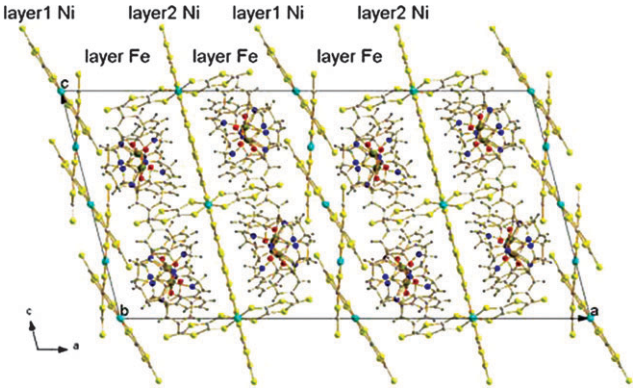

Fig. 4 Structure of *m*-**1**′ viewed along axis b.

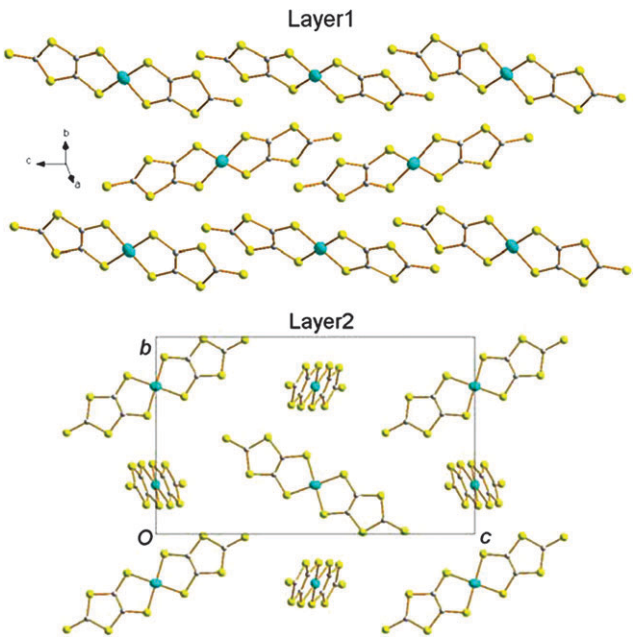

Fig. 5 Structural arrangement of layer1 Ni (top) and layer2 Ni (bottom) in *m*-**1**′.

of Ni and Fe complexes lying on the bc plane and alternating along the a direction (Fig. 4). The layers of Ni complexes are not equivalent, as shown by Fig. 5, top and bottom.

The layers of $[Fe(sal_2\text{-trien})]^+$ cations are equivalent, since they are built up on the two independent units found in the asymmetric unit. Their relative arrangement (Fig. 6) allows classical short contacts only, without any π–π overlaps.

The asymmetric unit of *t*-**1**′ contains one $[Fe(sal_2\text{-trien})]^+$ cation, one $[Ni(dmit)_2]^-$ anion, one $(CH_3)_2CO$ molecule and one CH_3CN molecule (Fig. 1). The structure of *t*-**1**′ can be described as layers of $[Ni(dmit)_2]^-$ units alternating along the c direction with mixed layers of $[Fe(sal_2\text{-trien})]^+$ and solvent molecules (Fig. 7). All layers are equivalent.

The asymmetric unit of *t*-**1**″ contains one $[Fe(sal_2\text{-trien})]^+$ cation, one $[Ni(dmit)_2]^-$ anion and one $(CH_3)_2CO$ molecule (Fig. 1). Like the structures of *t*-**1** and *m*-**1**, the structure of *t*-**1**″ can be described as double layers of $[Ni(dmit)_2]^-$ units separated from each other by a double layer of $[Fe(sal_2\text{-trien})]^+$ and

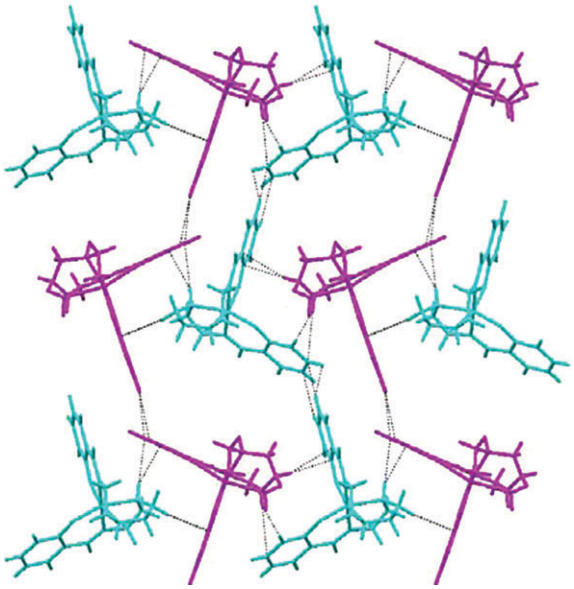

Fig. 6 Structural arrangement of the $[Fe(sal_2\text{-trien})]^+$ cations in the bc plane in *m*-**1**′ (dotted lines represent short contacts of less than the sum of the van der Waals radii).

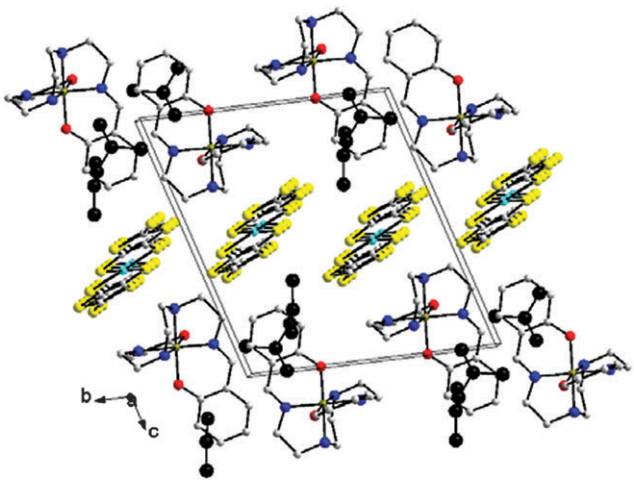

Fig. 7 View of *t*-**1**′ along the a axis (CH_3CN and $(CH_3)_2CO$ molecules are in black).

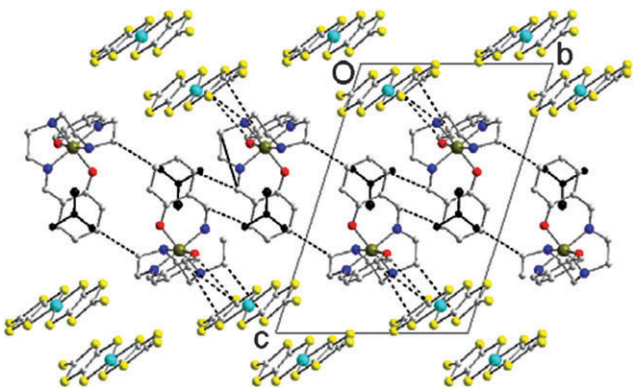

Fig. 8 Structure of *t*-**1**″ viewed along the a axis (dotted lines represent C–C contacts shorter than 3.6 Å).

$(CH_3)_2CO$ moieties, each layer spreading over the ab plane and alternating along the a direction (Fig. 8).

Due to the fact that *m*-**1**′ and *t*-**1**′ have only been synthesised in small amounts (produced by re-crystallization and not direct synthesis), their spectroscopic study is not discussed in this paper.

Magnetic properties: the effect of applied pressure on the materials

The magnetic properties of *t*-**1** were previously discussed,[14] and it was found that the complex undergoes a thermal SCO with hysteresis at atmospheric pressure. Unlike the triclinic polymorph, monoclinic *m*-**1** and triclinic *t*-**1**″ do not undergo a thermal spin transition; the former remains in the HS state and the latter remains in the LS state in the temperature range 4–300 K.

In ref. 27, an unusual behaviour induced by a low external applied pressure was reported for *t*-**1**. At 500 bar, the hysteresis loop became wider (*ca.* 61 K) and the transition was blocked at *ca.* 50% upon cooling, indicating a possible structural phase transition under pressure. In order to examine the effect of pressure on the monoclinic *m*-**1** polymorph of the $[Fe(sal_2\text{-trien})][Ni(dmit)_2]$ complex, magnetic susceptibility measurements were carried out under various hydrostatic pressures. These experiments revealed that even up to 3 kbar applied pressure, no thermal SCO took place in the 400–5 K temperature range; thus, the ferric entity remained in the HS state.

Spectroscopic studies

Mössbauer spectroscopy. The Mössbauer spectrum (see Fig. S1 in ESI†) of the triclinic $[Fe(sal_2\text{-trien})][Ni(dmit)_2]$ complex recorded at room temperature displays a doublet with hyperfine parameters $\delta = 0.36(1)$ mm s^{-1} and $\Delta E_Q = 0.53(2)$ mm s^{-1}, which are typical for a HS ferric species. The spectrum recorded at 80 K is very different from that recorded at 298 K; the quadrupole doublet displayed in the spectrum has hyperfine parameters of $\delta = 0.186(3)$ mm s^{-1} and $\Delta E_Q = 2.705(6)$ mm s^{-1}, characteristic for LS ferric compounds. The slight asymmetry of the spectra is due to a texture effect. This, as well as the lack of relaxation lines, has been previously discussed.[27]

The Mössbauer spectrum (see Fig. S1 in ESI†) of the monoclinic $[Fe(sal_2\text{-trien})[Ni(dmit)_2]$ complex recorded at room temperature, with hyperfine parameters of $\delta = 0.37(3)$ mm s^{-1} and $\Delta E_Q = 0.53(3)$ mm s^{-1}, is very similar to that of the triclinic polymorph. Indeed, the slight difference is within the error of the Mössbauer measurement, which is in agreement with the very similar ligand arrangements around the ferric ions. However, the spectrum of the monoclinic polymorph recorded at 80 K, with hyperfine parameters of $\delta = 0.50(1)$ mm s^{-1} and $\Delta E_Q = 0.60(2)$ mm s^{-1}, is very different from that of the triclinic polymorph since the former remains in the HS state and the triclinic polymorph undergoes a thermal spin transition above this temperature. The difference in the isomer shifts for the monoclinic polymorph is due to the second-order Doppler shift, and its value (0.13(4)) corresponds well to what is expected in this temperature range.

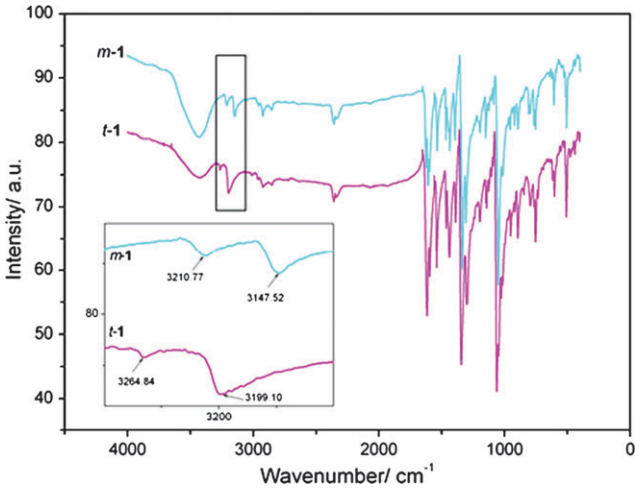

Fig. 9 IR spectra of *t*-**1** (purple line) and *m*-**1** (blue line) at 298 K.

Infrared spectroscopy. Room temperature infrared spectra (Fig. 9) of the triclinic and monoclinic [Fe(sal$_2$-trien)][Ni(dmit)$_2$] complexes display only two slight differences in their high wavenumber range. The spectrum of the triclinic polymorph displays two transmission bands at 3264.84 and 3199.10 cm^{-1}, whereas in the spectrum of the monoclinic polymorphs, these transmission bands are shifted by *ca.* 50 cm^{-1} to 3210.77 and 3147.52 cm^{-1}, respectively. The remaining spectra do not display such substantial discrepancies.

Raman spectroscopy. Numerous discrepancies can be found in the spectra of the triclinic polymorph at different temperatures (Fig. 10), in agreement with the thermal spin transition, as well as in the Raman spectra of the distinct polymorphs at room temperature (as well as at 80 K). The differences in the 1300–1500 cm^{-1} range are particularly apparent (see Fig. 11).

Apart from the peak at ~1400 cm^{-1}, assigned to the $A_g(1)$ C=C bond stretching mode in the [Ni(dmit)$_2$]$^-$ anion,[28] the C=C (aromatic) stretching modes (among others) that relate to the [Fe(sal$_2$-trien)][Ni(dmit)$_2$] complex appear in this region.

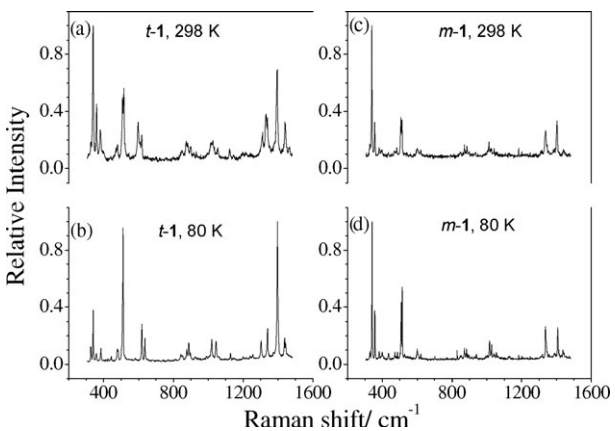

Fig. 10 Raman spectra of (a,b) *t*-**1** and (c,d) *m*-**1** recorded at (a,c) 298 K and (b,d) 80 K, respectively.

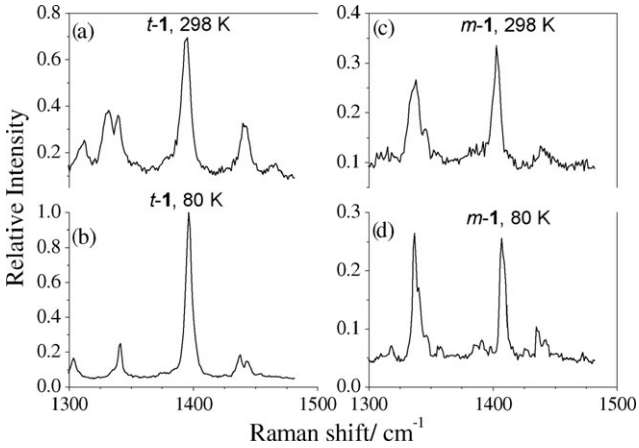

Fig. 11 Raman spectra of (a,b) *t*-**1** and (c,d) *m*-**1** recorded at (a,c) 298 K and (b,d) 80 K, respectively, in the 1300–1500 cm^{-1} range.

Discussion

As seen previously, the "disappearance" of polymorphs is not so uncommon.[24–26] We only obtained other phases, whatever the experimental conditions (concentration, temperature or time of addition, temperature of crystallization, *etc.*...). Although not the point of this article, this disappearance deserves a few words of explanation. A possible explanation of this phenomenon may lie in the nature of the [Fe(sal$_2$-trien)]PF$_6$ complex, since this starting salt was synthesised in a large quantity for the first time in our group by following the procedure described by Tweedle and Wilson.[29] This batch (characterized by elemental analysis and IR spectroscopy) allowed us to synthesize numerous batches of [Fe(sal$_2$-trien)][Ni(dmit)$_2$], which were reproduced many times by several people in our laboratory, and have always led to the formation of the SCO complex with the thermal hysteresis *t*-**1** polymorph as the unique phase. As communicated previously,[27] the so-obtained complex was used-up by physical and electrochemical experiments. Following on from this, new syntheses of [Fe(sal$_2$-trien)]PF$_6$ were carried out, but now without the triclinic phase being obtained. Therefore, the quality of this reactant seems to be crucial to the magnetic properties of the final product. Even when using some of the remaining seeds of the *t*-**1** phase, the various re-crystallizations led to one of the polymorphs or pseudo-polymorphs, depending on the solvent used.‡

The intramolecular bond distances and bond angles in the Ni-bearing complex are almost identical, whatever the temperature. This is not surprising, since [Ni(dmit)$_2$]$^-$ behaves here like a typical counter-ion, and its oxidation state and spin state do not change with temperature.

Unlike the *t*-**1** phase, none of these new polymorphs undergo thermal spin transition and all remain in the HS state, except for *t*-**1**″. Concerning the Fe-bearing entity, it is well known that the structural features of the Fe units of SCO complexes vary substantially as a function of their spin state. For instance, the bond lengths around ferric (and ferrous) ions are shorter in the LS state than in the HS state. The lack of discrepancies in the Fe cation between the structures at 295 and 180 K clearly shows that *m*-**1** always remains in the HS

state, whatever the temperature, in agreement with the magnetic measurements.

The very different magnetic properties, as a function of temperature and pressure, of the *t*-**1** and *m*-**1** polymorphs of the [Fe(sal_2-trien)][Ni($dmit)_2$] complex, as well as their similar intramolecular structures and very different intermolecular interactions, can also be described by a spectroscopic approach.

Mössbauer studies at 298 K did not show any discrepancies between the two polymorphs, since the HS structures and ligand arrangements around the ferric entities are very similar. This latter fact is not surprising since Mössbauer spectroscopy is a method that is very sensitive to the oxidation and spin state of Fe, as well as to the ligand arrangement around the Fe ions (including the nature of the ligands, coordination number, structural distortion, *etc*...). However, using Mössbauer spectroscopy, only the Fe entities, furthermore, only the immediate neighbourhood around the Fe entities, is probed, unless long range interactions (*i.e.* magnetic) are present in the material, which may further affect the resultant spectral pattern.

However, vibrational spectroscopy, apart from exhibiting fingerprint patterns for both major phases, displayed some differences in the resultant spectra of the triclinic and monoclinic polymorphs. Both, IR and Raman spectroscopy showed rather substantial differences in the spectra between the distinct phases, especially in regions where modes for aromatic vibrations are expected. In the IR spectra, the transmission bands displayed at *ca.* ~3210–3260 and ~3150–3200 cm^{-1} could be clearly assigned as the frequencies of aromatic C–H stretching vibration modes, which, in the case of the triclinic polymorph, are about 50 cm^{-1} higher than for the monoclinic polymorph. These lower energy values correspond very well to the observed strong π–π interactions in the case of the triclinic phase, where there is less room for C–H vibrations. In the case of Raman spectroscopy, complete assignment of spectra has not been undertaken. However, it is known that the C=C (aromatic) stretching modes (among others) appear in the 1300–1500 cm^{-1} region. Since all of these frequencies change as a function of the polymorph, it can be safely concluded that the differences in the π–π interactions of the distinct phases will appear in Raman spectra as well.

Careful examination of the intramolecular bond distances and angles reveal that only a few discrepancies exist between these complexes (Table S1 in ESI† and Table 2). The bond distances between the central Fe and the O/N atoms of the ligand are almost identical for *t*-**1** and *m*-**1**, since the largest differences are *ca.* 1% between them. Concerning the bond angles, discrepancies up to *ca.* 7% are found between the two polymorphs.

Table 2 Selected bond distances (Å) and angles (°), together with the largest discrepancies (%) observed in *t*-**1** and *m*-**1** at 293 and 295 K

	t-**1**	*m*-**1**	Δ (%)
Fe(1)–O(2)	1.919(2)	1.896(2)	−1.20
Fe(1)–N(4)	2.124(3)	2.104(2)	−0.94
O(1)–Fe(1)–N(4)	94.2(1)	100.78(8)	6.99
N(1)–Fe(1)–N(4)	178.3(1)	171.41(8)	−3.86
O(2)–Fe(1)–N(2)	89.8(1)	92.87(8)	3.42
N(4)–Fe(1)–N(2)	101.4(1)	95.22(8)	−6.09

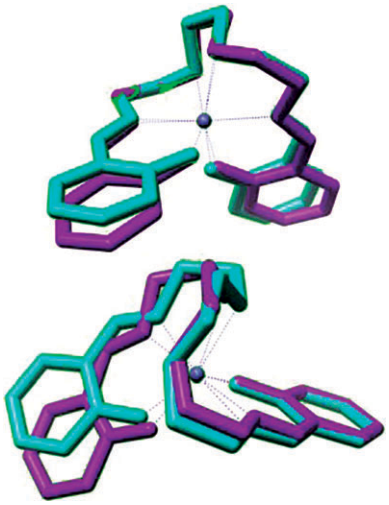

Fig. 12 Figures showing the non-superposition of the Fe complexes in *t*-**1** and *m*-**1**.

Despite these differences, the octahedral volume based on six coordinating atoms around the Fe is almost identical for both phases: 11.31 $Å^3$ for *t*-**1** and 11.21 $Å^3$ for *m*-**1**. Along the same lines, the angles between the three equatorial planes of the octahedron are almost identical (largest difference of 2.3%) (Table S2 in ESI†). The only noticeable feature lies in the angles between the opposite triangular faces of the octahedron; differences of up to *ca.* 30% are observed for the angles between the faces, O1–O2–N1 and N2–N3–N4, and also between O1–N3–N4 and N2–O2–N1.

These large differences result in the deformation of the octahedron around the Fe, which is reflected in Fig. 12. It is impossible to superimpose the whole Fe complex of *t*-**1** and *m*-**1**; in the best case (Fig. 12, top) the trien units of each polymorph are almost eclipsed, but neither sal rings are. On the other hand, superposing one of the sal rings results in the total distinction of the rest of the molecule (Fig. 12, bottom). This is due to the flexibility of the trien unit, which does not exhibit the same torsion angles in *t*-**1** as in *m*-**1**. There are also some discrepancies between the torsion angles (Table S3 in ESI†), with the two most important angles being N3–C12–C13–N4 and C14–N4–C13–C12; there being a difference of *ca.* 24° in the former, while the latter is counted as negative in *t*-**1** but positive in *m*-**1**. This shows that the orientation of the atoms bound either to either C14 or C12 is

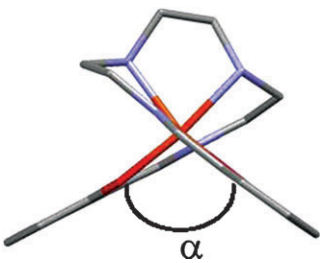

Fig. 13 A view of the Fe(sal_2-trien) complex with the representation of the α angle.

Table 3 Comparison of numerous geometrical parameters in *t*-**1**, *m*-**1**, *m*-**1′**, *t*-**1′** and *t*-**1″**

	T/K	Average Fe–N_{amine}	Average Fe–N_{imine}	Average Fe–O	Σ	θ	τ	α	Spin state	Ref.
t-**1**	293	2.189(3)	2.121(3)	1.909(2)	96.9	345	13.06; −6.47	106.9	HS[b]	14
	180	2.003(4)	1.929(3)	1.874(3)	40.3	99	5.84; 24.54	72.9	LS[b]	
m-**1**	290	2.185(2)	2.106(2)	1.899(2)	91.4	295	14.17; 2.44	116.2	HS[b]	This work
	180	2.186(2)	2.105(2)	1.900(2)	91.4	295	16.09; 2.44	118.0	HS[b]	
m-**1′**[a]	295	2.128(4)	2.071(5)	1.886(3)	81.2; 80.1	292.0; 284.0	1.64; −9.56 8.78; −4.54	95.2; 96.3	HS[c]	This work
	160	2.035(3)	1.978(3)	1.877(2)	53.3; 57.4	193.0; 163.0	7.76; −9.89 8.48; −8.36	96.0; 96.2	LS[c]	
t-**1′**	250	2.009(2)	1.926(2)	1.875(2)	51.1	137.0	−9.31; −14.71	75.3	LS[c]	This work
	100	2.006(5)	1.929(4)	1.871(4)	51.4	140.0	−9.64; −16.08	73.8	LS[c]	
t-**1″**	293	2.008(6)	1.932(5)	1.876(4)	50.2	135.0	13.65; 16.03	72.5	LS[d]	This work

[a] There are two independent Fe(sal_2-trien) moieties in this complex. [b] Spin state deduced from magnetic and Mössbauer experiments. [c] Spin state deduced from the geometrical parameters. [d] Spin state deduced from magnetic experiments.

opposite in *t*-**1** as in *m*-**1**, which clearly indicates large modifications in the geometry of the trien unit.

Other indices have been used by several authors[30–32] to quantify the distortions, such as Σ, θ,[31,32] and more recently τ and α (Fig. 13).[30] Σ measures local angular distortions around the central atom of the octahedron and θ defines the degree of trigonal distortion of the six coordinated atoms of the ligand (both indices would be 0 for an ideal octahedron). $\sum = \sum_{i=1}^{12} |90 - \alpha_i|$; $\theta = \sum_{i=1}^{24} |60 - \theta_i|$, where α_i are the 12 *cis*-angles around the Fe, θ_i are the 24 unique angles measured on projection of the two triangular faces of the octahedron along their pseudo-threefold axis, τ is the torsion angle Fe–O–C–C, which involves the phenoxide ligand (2 per Fe unit), and α is the dihedral angle between the least-squares planes of the two phenoxy rings.

In Table 3, the large values of Σ and θ again reflect a substantial distortion of the octahedron around the Fe in both complexes. The dihedral angles between the phenoxy groups are almost identical in *t*-**1** and *m*-**1**, but the opposite sign of τ in *t*-**1** compared to *m*-**1** indicates that the phenoxy groups do not rotate in the same direction about the Fe in these two complexes

Another point that deserves to be discussed concerns the number and nature of the short contacts (smaller than the sum of the van der Waals radii of the concerned atoms) within these polymorphs.

At first sight and numerically speaking, there are many more contacts in *m*-**1** (28) than in *t*-**1** (19) (Table S4 in ESI†). In *t*-**1**, these contacts involve five distinct Ni(dmit)$_2$ and seven distinct Fe(sal_2-trien) moieties, whereas seven Ni(dmit)$_2$ and nine distinct Fe(sal_2-trien) moieties are implied in the contacts within *m*-**1**. This seems quite contradictory to the magnetic behaviour observed in these complexes, since *t*-**1** exhibits a spin transition with a hysteresis, whereas *m*-**1** always remains in the HS state, whatever the temperature. Actually, a better picture might be given by considering the π–π contacts (or C–C contacts shorter than 3.6 Å) in both complexes (Table S5 in ESI†). By doing so, it appears that there are 17 contacts in *t*-**1** (ranging from 3.306(6) to 3.593(5) Å) involving four distinct Fe(sal_2-trien) moieties, whereas only four contacts are found in *m*-**1** (ranging from 3.385(4) to 3.596(5) Å), which implies only one Fe moiety. This is much more consistent with the HS–LS spin transition, the hysteresis observed in *t*-**1** and the constant HS state of *m*-**1**.

To conclude the comparison between *t*-**1** and *m*-**1** at 295 K, we can describe the similarities and differences between these complexes, but no quantitative considerations can be drawn from them, since we are not able to measure the effective strength of the contacts or confirm that any given interaction is more important than any other. Indeed, in *m*-**1**, like in [Fe(sal_2-trien)]ClO_4, there exists a dimerisation of Fe(sal_2-trien) moieties through four C–C contacts and more particularly through C5 and C7 (short distance of 3.385(4) Å; symmetry code $1 - x, -y, 1 - z$). Like in [Fe(sal_2-trien)]ClO_4, the rings are parallel at a distance of 3.09(1) Å. The other phenoxy group is also strongly bound to an adjacent Ni(dmit)$_2$ unit, resulting in a rigid structure that prevents changes in the conformation of the Fe(sal_2-trien) unit, and thus inhibits a possible SCO. This feature may be the source of the thermal SCO in *t*-**1** but not in *m*-**1**. Indeed, in *t*-**1**, the Fe unit is connected mainly to two Fe(sal_2-trien) units through π–π contacts, and to two others through classical short contacts to the flexible trien unit. The decrease of temperature leads to a shortening of the c axis, which implies that the aromatic rings move closer to each other. The increased repulsive interactions between the phenoxy rings is strong enough to induce their shift, leading to a re-arrangement of the Fe(sal_2-trien) unit to a different conformation and eventually to edge-to-edge π–π interactions.

Among these polymorphs, *t*-**1** is the only one that has been proved to undergo SCO with hysteresis centred around 250 K. In this complex, variations of the average bond lengths around the Fe atom, and large differences of Σ and θ between 290 and 180 K are thus not surprising, and confirm the more regular shape of the octahedron around Fe in the LS state than in the HS state. *m*-**1** has also been proven to remain in the HS state whatever the temperature. No discrepancy is observed for this complex.

Due to their very small extent, no magnetic studies could be performed on *m*-**1′** and *t*-**1′**. The lack of discrepancies of the values reported for *t*-**1′** at 250 and 100 K strongly suggests that it remains in the same spin state. The similarities of the average bond lengths of *t*-**1′** with those of *t*-**1** at 180 K and those of *t*-**1″** at 293 K indicate that *t*-**1′** is in the LS state. The low values of Σ and θ, and their similarities in *t*-**1′** and *t*-**1″**, are also in agreement with the same spin state (LS) for these two compounds. On the contrary, for *m*-**1′**, large discrepancies in

the values between 295 and 160 K can be seen for the averaged bond lengths Σ and θ. This strongly suggests that *m*-**1**′ could undergo a spin transition between these two temperatures. The values reported at 295 K are slightly smaller for *m*-**1**′ compared to *t*-**1**, suggesting that most of the Fe ions are in the HS state, whereas those at 160 K are slightly larger than those reported for *t*-**1** at 180 K, suggesting that most of the Fe ions are in the LS state. Unfortunately, as indicated above, this polymorph has only been obtained as a few crystals after re-crystallization of a native batch of *t*-**1**, which prevents any magnetic or Mössbauer experiments.

For all the compounds reported, regardless of their spin state, the value of α is either above or below 90°, indicating that this value is not necessarily of importance, but it is remarkable (see Table 3) that only the two polymorphs that undergo SCO (*t*-**1** and maybe *m*-**1**′) have τ values with different signs.

Conclusions

Four new polymorphs of the triclinic SCO [Fe(sal$_2$-trien)]-[Ni(dmit)$_2$] complex have been synthesized and characterised. None of them have been proven to undergo a spin transition. Nevertheless, although their crystal structures are not similar, several noticeable features have emerged from the analysis of their intra- and intermolecular geometries. In particular, both the torsion angles involving the phenoxy rings and the nature (π–π interactions) of the short contacts between the molecular moieties seem to be of major importance for the complexes to exhibit SCO. Attempts to synthesize the native phase *t*-**1**, as well as the new polymorph *m*-**1**′, are still in progress to confirm the trends observed in this work.

Experimental

Solvents were purified and distilled under argon. Syntheses were performed under an argon atmosphere. [Fe(sal$_2$-trien)]PF$_6$ and (*n*-Bu$_4$N)[Ni(dmit)$_2$] were synthesized using literature procedures.[29,33]

Synthesis of polymorph *m*-1

m-**1** was synthesised by the addition of a CH_3CN solution (15 mL) of (*n*-Bu$_4$N)[Ni(dmit)$_2$] (59 mg, 0.084 mmol) over a CH_3CN solution (3 mL) of [Fe(sal$_2$-trien)]PF$_6$ (85 mg, 0.153 mmol). The resulting solution was left at 4 °C overnight. After filtration, dark green crystals (plate or bar) (36 mg) were obtained, washed with CH_3CN and dried under a vacuum. Yield: 55%. Elemental analysis calc. for $C_{26}H_{24}FeN_4NiO_2S_{10}$: C, 36.32; H, 2.81; N, 6.52. Found: C, 36.12; H, 2.42; N, 6.28%.

Synthesis of polymorph *m*-1′

m-**1**′ was obtained as a couple of plates after the re-crystallization of a few crystals from a *t*-**1** batch in CH_3CN.

Synthesis of polymorph *t*-1′

t-**1**′ was obtained as thick plates after the re-crystallization of *m*-**1** from a mixture of $(CH_3)_2CO$ and CH_3CN.

Synthesis of polymorph *t*-1″

t-**1**″ was synthesised at −80 °C by the addition of a $(CH_3)_2CO$ solution (10 mL) of (*n*-Bu$_4$N)[Ni(dmit)$_2$] (121.8 mg, 0.175 mmol) over a $(CH_3)_2CO$ solution (8 mL) of [Fe(sal$_2$-trien)]PF$_6$ (97.6 mg, 0.177 mmol). The resulting solution was left standing at 20 °C overnight. After filtration, dark green crystals (block or plate) (76 mg) were obtained, washed with $(CH_3)_2CO$ and dried under a vacuum. Yield: 47%. Elemental analysis calc. for $C_{29}H_{30}FeN_4NiO_3S_{10}$: C, 37.95; H, 3.29; N, 6.10. Found: C, 36.92; H, 2.76; N, 6.04%.

X-Ray crystallography

The experimental details and crystal data are listed in Table 1. Data collection and cell refinement were performed with a sealed Mo-K$_\alpha$ (λ = 0.71073 Å) X-ray source on a STOE imaging plate diffraction system (IPDS) on an Oxford Xcalibur or Bruker Apex2 diffractometer, by using IPDS,[34] CrysAlis[35] or Bruker SMART[36] software, respectively. Data reduction was performed by using the IPDS,[34] Crysalis Red[37] or Bruker SAINT[36] programs. Details of the measurements for each structure can be found in the ESI cif files.† The structures were solved using SIR97[38] or SHELXS-97[39] and refined subsequently using SHELXL-97.[40] Calculations were carried out using the WinGX package program.[41] Drawings of the molecular structures were obtained using Diamond,[42] Mercury[43] or ORTEP.[44] The atomic scattering factors were taken from the International Tables for X-Ray Crystallography.[45]

Mössbauer spectroscopy

Mössbauer experiments were carried out in a flow-type liquid nitrogen cryostat using a conventional constant acceleration-type Mössbauer spectrometer. γ-rays were provided by a ^{57}Co(Rh) source (15 mCi). Spectral evaluations were performed with the assumption of Lorentzian line shapes using Recoil software.[46] All isomer shifts are given relative to α-Fe at room temperature.

Raman spectroscopy

Variable-temperature Raman spectra were collected in the 300–1600 cm^{-1} wavenumber range. Samples were enclosed under a nitrogen atmosphere on the cold finger of a THMS600 (Linkam) liquid nitrogen cryostage. Before measurements were taken, the samples were kept at 350 K for ~30 min in order to eliminate the possible residues of solvents. The LabRAM-HR (Jobin Yvon) Raman spectrometer used in these experiments consisted of a BXFM (Olympus) optical microscope, a single-grating spectrograph (1800 grooves mm^{-1}, f = 800 mm) and a DU420-OE (Andor) CCD detector. The entrance slit was kept at 100 mm and a spectral resolution of *ca.* 1 cm^{-1} was obtained. The 632.8 nm line of a 17 mW He/Ne laser was used as the excitation source, and plasma lines were removed by using a narrow-band interference filter. The exciting radiation was directed through a neutral density filter (OD = 2) to avoid sample heating and was focused onto the sample through a ×50, 10.6 mm working distance objective (NA = 0.5). The scattered light was collected in a backscattering configuration using the same microscope objective. Rayleigh scattering was removed by means of a holographic notch filter.

Infrared spectroscopy

Infrared spectra were recorded in the 4000–400 cm^{-1} wavenumber range using a Perkin-Elmer Spectrum™ 100 FT-IR spectrometer equipped with a universal ATR sampling accessory at room temperature.

Magnetic susceptibility measurements

Variable-temperature magnetic susceptibility measurements were carried out between 300 and 5 K on polycrystalline samples using a Quantum Design MPMS2 SQUID magnetometer operated at 1.0 T. The magnetometer was calibrated with $(NH_4)_2Mn(SO_4)_2{\cdot}12H_2O$. Experimental susceptibilities were corrected for diamagnetism of the constituent atoms by the use of Pascal's constants.

Experiments under pressure

Magnetic susceptibility measurements under high pressure were carried out in a magnetic field of 1 or 2 T for the monoclinic and triclinic polymorphs, respectively, using a clamp-type hardened beryllium bronze (CuBe) cell. Hydrostatic conditions were obtained by mixing the powder samples with a pressure-transmitting mineral oil. Details of the pressure cell are given elsewhere.[47]

Acknowledgements

The authors wish to thank M. Marchivie and P. Guionneau for providing the program used to calculate θ values, and M. Halcrow for useful discussions.

References

1 Spin Crossover in Transition Metal Compounds I–III, *Top. Curr. Chem.*, ed. P. Gütlich and H. A. Goodwin, 2004, vol. 233–235.
2 P. Gütlich, A. Hauser and H. Spiering, *Angew. Chem., Int. Ed. Engl.*, 1994, **33**, 2024.
3 A. Bousseksou, G. Molnar and G. Matouzenko, *Eur. J. Inorg. Chem.*, 2004, 4353.
4 J. A. Real, A. B. Gaspar and M. C. Muñoz, *Dalton Trans.*, 2005, 2062.
5 J. A. Real, A. B. Gaspar, V. Niel and M. C. Muñoz, *Coord. Chem. Rev.*, 2003, **236**, 121.
6 A. B. Gaspar, V. Ksenofontov, M. Seredyuk and P. Gütlich, *Coord. Chem. Rev.*, 2005, **249**, 2661.
7 Y. Garcia, V. Niel, M. C. Muñoz and J. A. Real, *Top. Curr. Chem.*, 2004, **233**, 229.
8 O. Kahn, J. Krober and C. Jay, *Adv. Mater.*, 1992, **4**, 718.
9 O. Kahn and C. Martinez-Jay, *Science*, 1998, **279**, 44.
10 J.-F. Letard, P. Guionneau and L. Goux-Capes, *Top. Curr. Chem.*, 2004, **235**, 221.
11 A. Bousseksou, G. Molnar, P. Demont and J. Menegotto, *J. Mater. Chem.*, 2003, **13**, 2069.
12 A. Galet, A. B. Gaspar, M. C. Muñoz, G. V. Bukin, G. Levchenko and J. A. Real, *Adv. Mater.*, 2005, **17**, 2949.
13 P. Cassoux and J. Miller, in *Chemistry of Advanced Materials: An Overview*, ed. L. V. Interrante and M. J. Hampden-Smith, Wiley-VCH, New York, USA, 1998, pp. 19–72.
14 S. Dorbes, L. Valade, J. A. Real and C. Faulmann, *Chem. Commun.*, 2005, 69.
15 C. Faulmann, S. Dorbes, J. A. Real and L. Valade, *J. Low Temp. Phys.*, 2006, **142**, 265.
16 H. Oshio, K. Kitazaki, J. Mishiro, N. Kato, Y. Maeda and Y. Takashima, *J. Chem. Soc., Dalton Trans.*, 1987, 1341.
17 S. Hayami, Z. Gu, H. Yoshiki, A. Fujishima and O. Sato, *J. Am. Chem. Soc.*, 2001, **123**, 11644.
18 S. Hayami, T. Kawahara, G. Juhasz, K. Kawamura, K. Uehashi, O. Sato and Y. Maeda, *J. Radioanal. Nucl. Chem.*, 2003, **255**, 443.
19 K. Takahashi, H. Cui, H. Kobayashi, E. Yasuaki and O. Sato, *Chem. Lett.*, 2005, **34**, 1240.
20 K. Takahashi, H.-B. Cui, Y. Okano, H. Kobayashi, Y. Einaga and O. Sato, *Inorg. Chem.*, 2006, **45**, 5739.
21 C. Faulmann, K. Jacob, S. Dorbes, S. Lampert, I. Malfant, M.-L. Doublet, L. Valade and J. A. Real, *Inorg. Chem.*, 2007, **46**, 8548.
22 C. Faulmann, S. Dorbes, S. Lampert, K. Jacob, B. Garreau de Bonneval, G. Molnar, A. Bousseksou, J. A. Real and L. Valade, *Inorg. Chim. Acta*, 2007, **360**, 3870.
23 P. J. van Koningsbruggen, Y. Maeda and H. Oshio, *Top. Curr. Chem.*, 2004, **233**, 259.
24 J. D. Dunitz and J. Bernstein, *Acc. Chem. Res.*, 1995, **28**, 193.
25 J. Bernstein and J.-O. Henck, *Cryst. Eng.*, 1998, **1**, 119–128.
26 W. C. McCrone, in *Physics and Chemistry of the Organic Solid State*, ed. D. Fox, M. M. Labes and A. Weissberger, New York, 1965, pp. 725–767.
27 P. A. Szilágyi, S. Dorbes, G. Molnár, J. A. Real, Z. Homonnay, C. Faulmann and A. Bousseksou, *J. Phys. Chem. Solids*, 2008, **69**, 2681.
28 K. I. Pokhodnya, C. Faulmann, I. Malfant, R. Andreu-Solano, P. Cassoux, A. Mlayah, D. Smirnov and J. Leotin, *Synth. Met.*, 1999, **103**, 2016.
29 M. F. Tweedle and L. J. Wilson, *J. Am. Chem. Soc.*, 1976, **98**, 4824.
30 R. Pritchard, S. A. Barrett, C. A. Kilner and M. A. Halcrow, *Dalton Trans.*, 2008, 3159.
31 J. K. McCusker, A. L. Rheingold and D. N. Hendrickson, *Inorg. Chem.*, 1996, **35**, 2100.
32 M. Marchivie, P. Guionneau, J. F. Letard and D. Chasseau, *Acta Crystallogr., Sect. B: Struct. Sci.*, 2005, **61**, 25.
33 G. Steimecke, H. J. Sieler, R. Kirmse and E. Hoyer, *Phosphorus Sulfur*, 1979, **7**, 49.
34 *IPDS version 2.86*, STOE & Cie GmbH, Darmstadt, Germany, 1996.
35 Xcalibur CCD system: *CrysAlis CCD, version 1.171.24*, Oxford Diffraction, Yarnton, UK, 2004.
36 *SMART and SAINT*, Bruker AXS Inc., Madison, Wisconsin, USA, 2001.
37 Xcalibur CCD system: *CrysAlis RED, version 1.171.24*, Oxford Diffraction, Yarnton, UK, 2004.
38 A. Altomare, M. C. Burla, M. Camalli, G. L. Cascarano, C. Giacovazzo, A. Guagliardi, A. G. G. Moliterni, G. Polidori and R. Spagna, *J. Appl. Crystallogr.*, 1999, **32**, 115.
39 G. M. Sheldrick, *SHELXS-97, Program for the solution of crystal structures*, University of Göttingen, Germany, 1997.
40 G. M. Sheldrick, *SHELXL-97, Program for the refinement of crystal structures*, University of Göttingen, Germany, 1997.
41 L. J. Farrugia, *J. Appl. Crystallogr.*, 1999, **32**, 837.
42 *Diamond version 3.1f*, Crystal Impact, Bonn, Germany, 2008.
43 *Mercury version 2.2*, Cambridge Crystallographic Data Centre, Cambridge, UK, 2001–2008 (http://www.ccdc.cam.ac.uk).
44 L. J. Farrugia, *J. Appl. Crystallogr.*, 1997, **30**, 565.
45 *International Tables for Crystallography*, ed. T. Hahn, Kluwer Academic Publishers, Dordrecht, The Netherlands, 1995, vol. A.
46 K. Lagarec and D. G. Rancourt, *Recoil*, Intelligent Scientific Applications Inc., Ottawa, ON, Canada, 1998.
47 G. Molnár, T. Guillon, N. O. Moussa, L. Rechignat, T. Kitazawa, M. Nardone and A. Bousseksou, *Chem. Phys. Lett.*, 2006, **423**, 152.

